
Unsupervised Learning of Lagrangian Dynamics from Images for Prediction and Control

Yaofeng Desmond Zhong
Princeton University
y.zhong@princeton.edu

Naomi Ehrich Leonard
Princeton University
naomi@princeton.edu

Abstract

Recent approaches for modelling dynamics of physical systems with neural networks enforce Lagrangian or Hamiltonian structure to improve prediction and generalization. However, when coordinates are embedded in high-dimensional data such as images, these approaches either lose interpretability or can only be applied to one particular example. We introduce a new unsupervised neural network model that learns Lagrangian dynamics from images, with interpretability that benefits prediction and control. The model infers Lagrangian dynamics on generalized coordinates that are simultaneously learned with a coordinate-aware variational autoencoder (VAE). The VAE is designed to account for the geometry of physical systems composed of multiple rigid bodies in the plane. By inferring interpretable Lagrangian dynamics, the model learns physical system properties, such as kinetic and potential energy, which enables long-term prediction of dynamics in the image space and synthesis of energy-based controllers.

1 Introduction

Humans can learn to predict the trajectories of mechanical systems, e.g., a basketball or a drone, from high-dimensional visual input, and learn to control the system, e.g., catch a ball or maneuver a drone, after a small number of interactions with those systems. We hypothesize that humans use domain-specific knowledge, e.g., physics laws, to achieve efficient learning. Motivated by this hypothesis, in this work, we propose incorporation of physics priors to learn and control dynamics from image data, aiming to gain interpretability and data efficiency. Specifically, we incorporate Lagrangian dynamics as the physic prior, which enables us to represent a broad class of physical systems. Recently, an increasing number of works [1, 2, 3, 4, 5] have incorporated Lagrangian/Hamiltonian dynamics into learning dynamical systems from coordinate data, to improve prediction and generalization. These approaches, however, require coordinate data, which are not always available in real-world applications. Hamiltonian Neural Network (HNN) [3] provides a single experiment with image observations, which requires a modification in the model. This modification is hard to generalize to systems with multiple rigid bodies. Hamiltonian Generative Network (HGN) [6] learns Hamiltonian dynamics from image sequences. However, the dimension of latent generalized coordinates is $4 \times 4 \times 16 = 256$, making interpretation difficult. Moreover, both HNN and HGN focus on prediction and have no design of control. Another class of approaches learn physical models from images, by either learning the map from images to coordinates with supervision on coordinate data [7] or learning the coordinates in an unsupervised way but only with translational coordinates [8, 9]. The unsupervised learning of rotational coordinates such as angles are under-explored in the literature.

In this work, we propose an unsupervised neural network model that learns coordinates and Lagrangian dynamics on those coordinates from images of physical systems in motion in the plane. The latent dynamical model enforces Lagrangian dynamics, which benefits long term prediction of the system. As Lagrangian dynamics commonly involve rotational coordinates to describe the changing

configurations of objects in the system, we propose a coordinate-aware variational autoencoder (VAE) that can infer interpretable rotational and translational coordinates from images without supervision. The interpretable coordinates together with the interpretable Lagrangian dynamics pave the way for introducing energy-based controllers of the learned dynamics.

1.1 Related work

Lagrangian/Hamiltonian prior in learning dynamics To improve prediction and generalization of physical system modelling, a class of approaches has incorporated the physics prior of Hamiltonian or Lagrangian dynamics into deep learning. Deep Lagrangian Network [1] and Lagrangian Neural Network [2] learn Lagrangian dynamics from position, velocity and acceleration data. Hamiltonian Neural Networks [3] learn Hamiltonian dynamics from position, velocity and acceleration data. By leveraging ODE integrators, Hamiltonian Graph Networks [10] and Symplectic ODE-Net [4] learn Hamiltonian dynamics from only position and velocity data. All of these works (except one particular experiment in HNN [3]) require direct observation of low dimensional position and velocity data. Hamiltonian Generative Network [6] learns Hamiltonian dynamics from images.

Unsupervised learning of dynamics We assume we are given no coordinate data and aim to learn coordinates and dynamics in an unsupervised way. With little position and velocity data, Belbute-Peres et al. [11] learn underlying dynamics. However, the authors observe that their model fails to learn meaningful dynamics when there is no supervision on position and velocity data at all. Without supervision, Watter et al. [12] and Levine et al. [13] learn locally linear dynamics and Jaques et al. [14] learns unknown parameters in latent dynamics with a given form. Kossen et al. [15] extracts position and velocity of each object from videos and learns the underlying dynamics. Watters et al. [16] adopts an object-oriented design to gain data efficiency and robustness. Battaglia et al. [17], Sanchez-Gonzalez et al. [18] and Watters et al. [7] learn dynamics with supervision by taking into account the prior of objects and their relations. These object-oriented designs focus little on rotational coordinates. Variational Integrator Network [19] considers rotational coordinates but cannot handle systems with multiple rotational coordinates.

Neural visual control Besides learning dynamics for prediction, we would like to learn how control input influences the dynamics and to design control laws based on the learned model. This goal is relevant to neural motion planning and model-based reinforcement learning from images. PlaNet [20] learns latent dynamical models from images and designs control input by fast planning in the latent space. Kalman VAE [21] can potentially learn locally linear dynamics and control from images, although no control result has been shown. Dreamer [22] is a scalable reinforcement learning agent which learns from images using a world model. Ebert et al. [23] propose a self-supervised model-based method for robotic control. We leave the comparison of our energy-based control methods and these model-based control methods in the literature to future work.

1.2 Contribution

The main contribution of this work is two-fold. First, we introduce an unsupervised learning framework to learn Lagrangian dynamics from image data for prediction. The Lagrangian prior conserves energy with no control applied; this helps learn more accurate dynamics as compared to a MLP dynamical model. Moreover, the coordinate-aware VAE in the proposed learning framework infers interpretable latent rigid body coordinates in the sense that a coordinate encoded from an image of a system in a position with high potential energy has a high learned potential energy, and vice versa. This interpretability enables us to design energy-based controllers to control physical systems to target positions. We implement this work with PyTorch [24] and refactor our code into PyTorch Lightning format [25], which makes our code easy to read and our results easy to reproduce. The code for all experiments is available at https://github.com/DesmondZhong/Lagrangian_caVAE.

2 Preliminary concepts

2.1 Lagrangian dynamics

Lagrangian dynamics are a reformulation of Newton’s second law of motion. The configuration of a system in motion at time t is described by generalized coordinates $\mathbf{q}(t) = (q_1(t), q_2(t), \dots, q_m(t))$,

where m is the number of degrees of freedom (DOF) of the system. For planar rigid body systems with n rigid bodies and k holonomic constraints, the DOF is $m = 3n - k$. From D'Alembert's principle, the equations of motion of the system, also known as the Euler-Lagrange equation, are

$$\frac{d}{dt} \left(\frac{\partial L}{\partial \dot{\mathbf{q}}} \right) - \frac{\partial L}{\partial \mathbf{q}} = \mathbf{Q}^{nc}, \quad (1)$$

where the scalar function $L(\mathbf{q}, \dot{\mathbf{q}})$ is the Lagrangian, $\dot{\mathbf{q}} = d\mathbf{q}/dt$, and \mathbf{Q}^{nc} is a vector of non-conservative generalized forces. The Lagrangian $L(\mathbf{q}, \dot{\mathbf{q}})$ is the difference between kinetic energy $T(\mathbf{q}, \dot{\mathbf{q}})$ and potential energy $V(\mathbf{q})$. For rigid body systems, the Lagrangian is

$$L(\mathbf{q}, \dot{\mathbf{q}}) = T(\mathbf{q}, \dot{\mathbf{q}}) - V(\mathbf{q}) = \frac{1}{2} \dot{\mathbf{q}}^T \mathbf{M}(\mathbf{q}) \dot{\mathbf{q}} - V(\mathbf{q}), \quad (2)$$

where $\mathbf{M}(\mathbf{q})$ is the mass matrix. In this work, we assume that the control inputs are the only non-conservative generalized forces, i.e., $\mathbf{Q}^{nc} = \mathbf{g}(\mathbf{q})\mathbf{u}$, where $\mathbf{g}(\mathbf{q})$ is the input matrix and \mathbf{u} is a vector of control inputs such as forces or torques. Substituting $\mathbf{Q}^{nc} = \mathbf{g}(\mathbf{q})\mathbf{u}$ and $L(\mathbf{q}, \dot{\mathbf{q}})$ from (2) into (1), we get the equations of motion in the form of m second-order ordinary differential equations (ODE):

$$\ddot{\mathbf{q}} = \mathbf{M}^{-1}(\mathbf{q}) \left(-\frac{d\mathbf{M}(\mathbf{q})}{dt} \dot{\mathbf{q}} + \frac{1}{2} \frac{\partial}{\partial \mathbf{q}} (\dot{\mathbf{q}}^T \mathbf{M}(\mathbf{q}) \dot{\mathbf{q}}) - \frac{dV(\mathbf{q})}{d\mathbf{q}} + \mathbf{g}(\mathbf{q})\mathbf{u} \right).^1 \quad (3)$$

2.2 Control via energy shaping

Our goal is to control the system to a reference configuration \mathbf{q}^* , inferred from a goal image \mathbf{x}^* , based on the learned dynamics. As we are essentially learning the kinetic and potential energy associated with the system, we can leverage the learned energy for control by *energy shaping* [26, 27].

If $\text{rank}(\mathbf{g}(\mathbf{q})) = m$, we have control over every DOF and the system is fully actuated. For such systems, control to the reference configuration \mathbf{q}^* can be achieved with the control law $\mathbf{u}(\mathbf{q}, \dot{\mathbf{q}}) = \boldsymbol{\beta}(\mathbf{q}) + \mathbf{v}(\dot{\mathbf{q}})$, where $\boldsymbol{\beta}(\mathbf{q})$ is the *potential energy shaping* and $\mathbf{v}(\dot{\mathbf{q}})$ is the *damping injection*. The goal of potential energy shaping is to let the system behave as if it is governed by a desired Lagrangian L_d with no non-conservative generalized forces.

$$\frac{d}{dt} \left(\frac{\partial L}{\partial \dot{\mathbf{q}}} \right) - \frac{\partial L}{\partial \mathbf{q}} = \mathbf{g}(\mathbf{q})\boldsymbol{\beta}(\mathbf{q}) \iff \frac{d}{dt} \left(\frac{\partial L_d}{\partial \dot{\mathbf{q}}} \right) - \frac{\partial L_d}{\partial \mathbf{q}} = 0, \quad (4)$$

where the desired Lagrangian has desired potential energy $V_d(\mathbf{q})$:

$$L_d(\mathbf{q}, \dot{\mathbf{q}}) = T(\mathbf{q}, \dot{\mathbf{q}}) - V_d(\mathbf{q}) = \frac{1}{2} \dot{\mathbf{q}}^T \mathbf{M}(\mathbf{q}) \dot{\mathbf{q}} - V_d(\mathbf{q}). \quad (5)$$

The difference between L_d and L is the difference between V and V_d , which explains the name potential energy shaping: $\boldsymbol{\beta}(\mathbf{q})$ shapes the potential energy V of the original system into a desired potential energy V_d . The potential energy V_d is designed to have a global minimum at \mathbf{q}^* . By the equivalence (4), we get

$$\boldsymbol{\beta}(\mathbf{q}) = \mathbf{g}^T (\mathbf{g}\mathbf{g}^T)^{-1} \left(\frac{\partial V}{\partial \mathbf{q}} - \frac{\partial V_d}{\partial \mathbf{q}} \right). \quad (6)$$

With only potential energy shaping, the system dynamics will oscillate around \mathbf{q}^* .² The purpose of damping injection $\mathbf{v}(\dot{\mathbf{q}})$ is to impose convergence, exponentially in time, to \mathbf{q}^* . The damping injection has the form

$$\mathbf{v}(\dot{\mathbf{q}}) = -\mathbf{g}^T (\mathbf{g}\mathbf{g}^T)^{-1} (\mathbf{K}_d \dot{\mathbf{q}}). \quad (7)$$

For underactuated systems, however, this controller design is not valid since $\mathbf{g}\mathbf{g}^T$ will not be invertible. In general, we also need kinetic energy shaping [27] to achieve a control goal.

¹In the 2020 NeurIPS Proceedings, there is an error in Equation (3), which is corrected here. The main results and conclusion of the paper are not affected – please see our Github repo https://github.com/DesmondZhong/Lagrangian_caVAE. We thank Rembert Daems for spotting the error in Equation (3).

²Please see Supplementary Materials for more details.

Remark The design parameters here are V_d and \mathbf{K}_d . A quadratic desired potential energy

$$V_d(\mathbf{q}) = \frac{1}{2}(\mathbf{q} - \mathbf{q}^*)^T \mathbf{K}_p(\mathbf{q} - \mathbf{q}^*), \quad (8)$$

results in a controller design

$$\mathbf{u}(\mathbf{q}, \dot{\mathbf{q}}) = \mathbf{g}^T (\mathbf{g}\mathbf{g}^T)^{-1} \left(\frac{\partial V}{\partial \mathbf{q}} - \mathbf{K}_p(\mathbf{q} - \mathbf{q}^*) - \mathbf{K}_d \dot{\mathbf{q}} \right). \quad (9)$$

This can be interpreted as a proportional-derivative (PD) controller with energy compensation.

2.3 Training Neural ODE with constant control

The Lagrangian dynamics can be formulated as a set of first-order ODE

$$\dot{\mathbf{s}} = \mathbf{f}(\mathbf{s}, \mathbf{u}), \quad (10)$$

where \mathbf{s} is a state vector and unknown vector field \mathbf{f} , which is a vector-valued function, can be parameterized with a neural network \mathbf{f}_ψ . We leverage Neural ODE, proposed by Chen et al. [28], to learn the function \mathbf{f} that explains the trajectory data of \mathbf{s} . The idea is to predict future states from an initial state by integrating the ODE with an ODE solver. As all the operations in the ODE solver are differentiable, \mathbf{f}_ψ can be updated by back-propagating through the ODE solver and approximating the true \mathbf{f} . However, Neural ODE cannot be applied to (10) directly since the input dimension and the output dimension of \mathbf{f} are not the same. Zhong et al. [4] showed that if the control remains constant for each trajectory in the training data, Neural ODE can be applied to the following augmented ODE:

$$\begin{pmatrix} \dot{\mathbf{s}} \\ \dot{\mathbf{u}} \end{pmatrix} = \begin{pmatrix} \mathbf{f}_\psi(\mathbf{s}, \mathbf{u}) \\ \mathbf{0} \end{pmatrix} = \tilde{\mathbf{f}}_\psi(\mathbf{s}, \mathbf{u}). \quad (11)$$

With a learned \mathbf{f}_ψ , we can apply a controller design $\mathbf{u} = \mathbf{u}(\mathbf{s})$ that is not constant, e.g., an energy-based controller, by integrating the ODE $\dot{\mathbf{s}} = \mathbf{f}(\mathbf{s}, \mathbf{u}(\mathbf{s}))$.

3 Model architecture

Let $\mathbf{X} = ((\mathbf{x}^0, \mathbf{u}^c), (\mathbf{x}^1, \mathbf{u}^c), \dots, (\mathbf{x}^{T_{\text{pred}}}, \mathbf{u}^c))$ be a given sequence of image and control pairs, where \mathbf{x}^τ , $\tau = 0, 1, \dots, T_{\text{pred}}$, is the image of the trajectory of a rigid-body system under constant control \mathbf{u}^c at time $t = \tau\Delta t$. From \mathbf{X} we want to learn a state-space model (10) that governs the time evolution of the rigid-body system dynamics. We assume the number of rigid bodies n is known and the segmentation of each object in the image is given. Each image can be written as $\mathbf{x}^\tau = (\mathbf{x}_1^\tau, \dots, \mathbf{x}_n^\tau)$, where $\mathbf{x}_i^\tau \in \mathbb{R}^{n_x}$ contains visual information about the i th rigid body at $t = \tau\Delta t$ and n_x is the dimension of the image space.

In Section 3.1, we parameterize $\mathbf{f}(\mathbf{s}, \mathbf{u})$ with a neural network and design the architecture of the neural network such that (10) is constrained to follow Lagrangian dynamics, where the physical properties such as mass and potential energy are learned from data. Since we have no access to state data, we need to infer states \mathbf{s} , i.e., generalized coordinates and velocities from image data. Sections 3.2 and 3.4 introduce an inference model (encoder) and a generative model (decoder) pair. Together they make up a variational autoencoder (VAE) [29] to infer the generalized coordinates in an unsupervised way. Section 3.3 introduces a simple estimator of velocity from learned generalized coordinates. The VAE and the state-space model are trained together, as described in Section 3.5. The model architecture is shown in Figure 1.

3.1 Latent Lagrangian dynamics

The Lagrangian dynamics (3) yield a second-order ODE. From a model-based perspective, they can be re-written as a first-order ODE (10) by choosing the state as $\mathbf{s} = (\mathbf{q}, \dot{\mathbf{q}})$. However, from a data-driven perspective, this choice of state is problematic when the generalized coordinates involve angles. Consider the pendulum task in Figure 2 as an example where we want to infer the generalized coordinate, i.e., the angle of the pendulum ϕ , from an image of the pendulum. The map from the image to the angle ϕ should be bijective. However, if we choose the state as $\mathbf{s} = (\phi, \dot{\phi})$, the map is not bijective, since ϕ and $\phi + 2\pi$ map to the same image. If we restrict $\phi \in [-\pi, \pi)$, then the

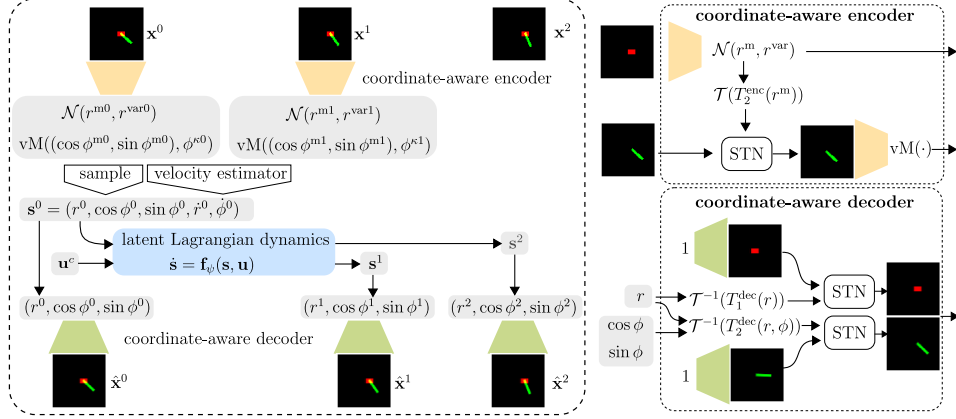


Figure 1: **Left:** Model architecture. (Using CartPole as an illustrative example.) The initial state \mathbf{s}^0 is constructed by sampling the distribution and a velocity estimator. The latent Lagrangian dynamics take \mathbf{s}^0 and the constant control \mathbf{u}^c for that trajectory and predict future states up to T_{pred} . The diagram shows the $T_{\text{pred}} = 2$ case. **Top-right:** The coordinate-aware encoder estimates the distribution of generalized coordinates. **Bottom-right:** The initial and predicted generalized coordinates are decoded to the reconstruction images with the coordinate-aware decoder.

dynamics are not continuous when the pendulum moves around the inverted position. Inspired by Zhong et al. [4], we solve this issue by proposing the state as $\mathbf{s} = (\cos \phi, \sin \phi, \dot{\phi})$, such that the mapping from the pendulum image to $(\cos \phi, \sin \phi)$ is bijective.

In general, for a planar rigid-body system with $\mathbf{q} = (\mathbf{r}, \phi)$, where $\mathbf{r} \in \mathbb{R}^{m_R}$ are translational generalized coordinates and $\phi \in \mathbb{T}^{m_T}$ are rotational generalized coordinates, the proposed state is $\mathbf{s} = (\mathbf{s}_1, \mathbf{s}_2, \mathbf{s}_3, \mathbf{s}_4, \mathbf{s}_5) = (\mathbf{r}, \cos \phi, \sin \phi, \dot{\mathbf{r}}, \dot{\phi})$, where \cos and \sin are applied element-wise to ϕ . To enforce Lagrangian dynamics in the state-space model, we take the derivative of \mathbf{s} with respect to t and substitute in (3) to get

$$\dot{\mathbf{s}} = \begin{pmatrix} \mathbf{s}_4 \\ -\mathbf{s}_3 \circ \mathbf{s}_5 \\ \mathbf{s}_2 \circ \mathbf{s}_5 \\ \mathbf{M}^{-1}(\mathbf{s}_1, \mathbf{s}_2, \mathbf{s}_3) \left(-\frac{1}{2} \frac{d\mathbf{M}(\mathbf{s}_1, \mathbf{s}_2, \mathbf{s}_3)}{dt} \begin{pmatrix} \mathbf{s}_4 \\ \mathbf{s}_5 \end{pmatrix} + \begin{pmatrix} -\frac{\partial V(\mathbf{s}_1, \mathbf{s}_2, \mathbf{s}_3)}{\partial \mathbf{s}_1} \\ \frac{\partial V(\mathbf{s}_1, \mathbf{s}_2, \mathbf{s}_3)}{\partial \mathbf{s}_2} \mathbf{s}_3 - \frac{\partial V(\mathbf{s}_1, \mathbf{s}_2, \mathbf{s}_3)}{\partial \mathbf{s}_3} \mathbf{s}_2 \end{pmatrix} + \mathbf{g}(\mathbf{s}_1, \mathbf{s}_2, \mathbf{s}_3) \mathbf{u} \right) \end{pmatrix} \quad (12)$$

where \circ is the element-wise product. We use three neural networks, $\mathbf{M}_{\psi_1}(\mathbf{s}_1, \mathbf{s}_2, \mathbf{s}_3)$, $V_{\psi_2}(\mathbf{s}_1, \mathbf{s}_2, \mathbf{s}_3)$, and $\mathbf{g}_{\psi_3}(\mathbf{s}_1, \mathbf{s}_2, \mathbf{s}_3)$, to approximate the mass matrix, the potential energy and the input matrix, respectively. Equation (12) is then a state-space model parameterized by a neural network $\dot{\mathbf{s}} = \mathbf{f}_{\psi}(\mathbf{s}, \mathbf{u})$. It can be trained as stated in Section 2.3 given the initial condition $\mathbf{s}^0 = (\mathbf{r}^0, \cos \phi^0, \sin \phi^0, \dot{\mathbf{r}}^0, \dot{\phi}^0)$ and \mathbf{u}^c . Next, we present the means to infer \mathbf{s}^0 from the given images.

3.2 Coordinate-aware encoder

From a latent variable modelling perspective, an image \mathbf{x} of a rigid-body system can be generated by first specifying the values of the generalized coordinates and then assigning values to pixels based on the generalized coordinates with a generative model - the decoder. In order to infer those generalized coordinates from images, we need an inference model - the encoder. We perform variational inference with a coordinate-aware VAE.

The coordinate-aware encoder infers a distribution on the generalized coordinates. The Gaussian distribution is the default for modelling latent variables in VAE. This is appropriate for modelling a translational generalized coordinate r since r resides in \mathbb{R}^1 . However, this is not appropriate for modelling a rotational generalized coordinate ϕ since a Gaussian distribution is not a distribution on \mathbb{S}^1 . If we use a Gaussian distribution to model hyperspherical latent variables, the VAE performs worse than a traditional autoencoder [30]. Thus, to model ϕ , we use the von Mises (vM) distribution, a family of distributions on \mathbb{S}^1 . Analogous to a Gaussian distribution, a von Mises distribution is

characterized by two parameters: $\mu \in \mathbb{R}^2$, $\|\mu\|^2 = 1$ is the mean, and $\kappa \in \mathbb{R}_{\geq 0}$ is the concentration around μ . The von Mises distribution reduces to a uniform distribution when $\kappa = 0$.

In our model, for a rotational generalized coordinate ϕ , we assume a posterior distribution $Q(\phi|\mathbf{x}) = \text{vM}((\cos \phi^m, \sin \phi^m), \phi^\kappa)$ with prior $P(\phi) = \text{vM}(\cdot, 0) = U(\mathbb{S}^1)$. For a translational generalized coordinate r , we assume a posterior distribution $Q(r|\mathbf{x}) = \mathcal{N}(r^m, r^{\text{var}})$ with prior $\mathcal{N}(0, 1)$. We denote the joint posterior distribution as $Q(\mathbf{q}|\mathbf{x})$ and joint prior distribution as $P(\mathbf{q})$. The encoder is a neural network that takes an image as input and provides the parameters of the distributions as output. A black-box neural network encoder would not be able to learn interpretable generalized coordinates for a system in motion described by Lagrangian dynamics. Instead, we propose a coordinate-aware encoder by designing the architecture of the neural network to account for the geometry of the system. This is the key to interpretable encoding of generalized coordinates.

Recall that each generalized coordinate q_j specifies the position/rotation of a rigid body i_j in the system. In principle, the coordinate can be learned from the image segmentation of i_j . However, the reference frame of a generalized coordinate might depend on other generalized coordinates and change across images. Take the CartPole example in Figure 2 as motivation. The system has two DOF and

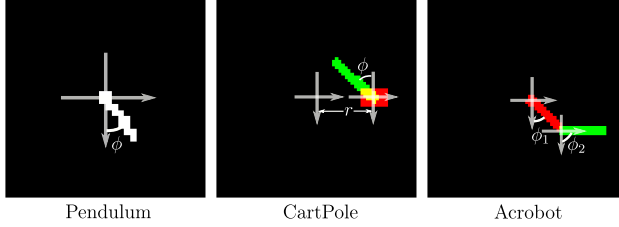


Figure 2: One choice of generalized coordinates and their corresponding reference frames in three example systems

natural choices of generalized coordinates are the horizontal position of the cart $q_1 = r$ and the angle of the pole $q_2 = \phi$. The origin of the reference frame of r is the center of the image, which is the same across all images. The origin of the reference frame of ϕ , however, is the center of the cart, which is not the same across all the images since the cart can move. In order to learn the angle of the pole, we can either use a translation invariant architecture such as Convolution Neural Networks (CNN) or place the center of the encoding attention window of the pole segmentation image at the center of the cart. The former approach does not work well in extracting generalized coordinates.³ Thus, we adopt the latter approach, where we shift our encoding attention window horizontally with direction and magnitude given by generalized coordinate r , before feeding it into a neural network to learn ϕ . In this way we exploit the geometry of the system in the encoder.

The default attention window is the image grid and corresponds to the default reference frame, where the origin is at the center of the image with horizontal and vertical axes. The above encoding attention window mechanism for a general system can be formalized by considering the transformation from the default reference frame to the reference frame of each generalized coordinate. The transformation of a point (x_d, y_d) in the default reference frame to a point (x_t, y_t) in the target reference frame is captured by transformation $\mathcal{T}(x, y, \theta)$ corresponding to translation by (x, y) and rotation by θ as follows:

$$\begin{pmatrix} x_t \\ y_t \\ 1 \end{pmatrix} = \mathcal{T}(x, y, \theta) \begin{pmatrix} x_d \\ y_d \\ 1 \end{pmatrix}, \quad \text{where} \quad \mathcal{T}(x, y, \theta) = \begin{pmatrix} \cos \theta & \sin \theta & x \\ -\sin \theta & \cos \theta & y \\ 0 & 0 & 1 \end{pmatrix}. \quad (13)$$

So let $\mathcal{T}((x, y, \theta)_j^{\text{enc}})$ be the transformation from default frame to reference frame of generalized coordinate q_j . This transformation might depend on constant parameters \mathbf{c} associated with the shape and size of the rigid bodies and generalized coordinates \mathbf{q}_{-j} , which denotes the vector of generalized coordinates with q_j removed. Let $(x, y, \theta)_j^{\text{enc}} = T_j^{\text{enc}}(\mathbf{q}_{-j}, \mathbf{c})$. Both \mathbf{q}_{-j} and \mathbf{c} are learned from images. However, the function T_j^{enc} is specified by leveraging the geometry of the system. In the CartPole example, $(q_1, q_2) = (r, \phi)$, and $T_1^{\text{enc}} \equiv (0, 0, 0)$ and $T_2^{\text{enc}}(q_1) = (q_1, 0, 0)$. In the Acrobot example, $(q_1, q_2) = (\phi_1, \phi_2)$, and $T_1^{\text{enc}} \equiv (0, 0, 0)$ and $T_2^{\text{enc}}(q_1, l_1) = (l_1 \sin q_1, l_1 \cos q_1, 0)$.

The shift of attention window can be implemented with a spatial transformer network (STN) [32], which generates a transformed image $\tilde{\mathbf{x}}_{i_j}$ from \mathbf{x}_{i_j} , i.e., $\tilde{\mathbf{x}}_{i_j} = \text{STN}(\mathbf{x}_{i_j}, \mathcal{T}(T_j^{\text{enc}}(\mathbf{q}_{-j}, \mathbf{c})))$. In general, to encode q_j , we use a multilayer perceptron (MLP) that takes $\tilde{\mathbf{x}}_{i_j}$ as input and provides the

³Here we expect to encode the angle of the pole from a pole image regardless of where it appears in the image. As the translation invariance of CNN is shown by Kauderer-Abrams [31] to be primarily dependent on data augmentation, the encoding of generalized coordinates might not generalize well to unseen trajectories. Also, in general we need both translation invariance and rotation invariance, a property that CNN do not have.

parameters of the q_j distribution as output. For a translational coordinate q_j , we have $(q_j^m, \log q_j^{\text{var}}) = \text{MLP}_j^{\text{enc}}(\tilde{\mathbf{x}}_{i_j})$. For a rotational coordinate q_j , we have $(\alpha_j, \beta_j, \log q_j^{\kappa}) = \text{MLP}_j^{\text{enc}}(\tilde{\mathbf{x}}_{i_j})$, where the mean of the von Mises distribution is computed as $(\cos q_j^m, \sin q_j^m) = (\alpha_j, \beta_j) / \sqrt{\alpha_j^2 + \beta_j^2}$. We then take a sample from the q_j distribution.⁴ Doing this for every generalized coordinate q_j , we can get $(\mathbf{r}^\tau, \cos \phi^\tau, \sin \phi^\tau)$ from \mathbf{x}^τ for any τ .⁵ We will use $(\mathbf{r}^0, \cos \phi^0, \sin \phi^0)$ and $(\mathbf{r}^1, \cos \phi^1, \sin \phi^1)$.

3.3 Velocity estimator

To integrate Equation (12), we also need to infer $(\dot{\mathbf{r}}^0, \dot{\phi}^0)$, the initial velocity. We can estimate the initial velocity from the encoded generalized coordinates by finite difference. We use the following simple first-order finite difference estimator:

$$\dot{\mathbf{r}}^0 = (\mathbf{r}^{\text{m}1} - \mathbf{r}^{\text{m}0}) / \Delta t, \quad (14)$$

$$\dot{\phi}^0 = ((\sin \phi^{\text{m}1} - \sin \phi^{\text{m}0}) \circ \cos \phi^{\text{m}0} - (\cos \phi^{\text{m}1} - \cos \phi^{\text{m}0}) \circ \sin \phi^{\text{m}0}) / \Delta t, \quad (15)$$

where $(\mathbf{r}^{\text{m}0}, \cos \phi^{\text{m}0}, \sin \phi^{\text{m}0})$ and $(\mathbf{r}^{\text{m}1}, \cos \phi^{\text{m}1}, \sin \phi^{\text{m}1})$ are the means of the generalized coordinates encoded from the image at time $t = 0$ and $t = \Delta t$, respectively. Jaques et al. [14] proposed to use a neural network to estimate velocity. From our experiments, our simple estimator works better than a neural network estimator.

3.4 Coordinate-aware decoder

The decoder provides a distribution $P(\mathbf{x}|\mathbf{q}) = \mathcal{N}(\hat{\mathbf{x}}, \mathbf{I})$ as output, given a generalized coordinate \mathbf{q} as input, where the mean $\hat{\mathbf{x}}$ is the reconstruction image of the image data \mathbf{x} . Instead of using a black box decoder, we propose a coordinate-aware decoder. The coordinate-aware decoder first generates a static image \mathbf{x}_i^c of every rigid body i in the system, at a default position and orientation, using a MLP with a constant input, i.e., $\mathbf{x}_i^c = \text{MLP}_i^{\text{dec}}(1)$. The coordinate-aware decoder then determines $\hat{\mathbf{x}}_i$, the image of rigid body i positioned and oriented on the image plane according to the generalized coordinates. The proposed decoder is inspired by the coordinate-consistent decoder by Jaques et al. [14]. However, the decoder of [14] cannot handle a system of multiple rigid bodies with constraints such as the Acrobot and the CartPole, whereas our coordinate-aware decoder can.

As in Jaques et al. [14], to find $\hat{\mathbf{x}}_i$ we use the inverse transformation matrix $\mathcal{T}^{-1}((x, y, \theta)_i^{\text{dec}})$ where \mathcal{T} is given by (13) and $(x, y, \theta)_i^{\text{dec}} = T_i^{\text{dec}}(\mathbf{q}, \mathbf{c})$. In the CartPole example, $(q_1, q_2) = (r, \phi)$, and $T_1^{\text{dec}}(r) = (r, 0, 0)$ and $T_2^{\text{dec}}(r, \phi) = (r, 0, \phi)$. In the Acrobot example, $(q_1, q_2) = (\phi_1, \phi_2)$, and $T_1^{\text{dec}}(\phi_1) = (0, 0, \phi_1)$ and $T_2^{\text{dec}}(\phi_1, \phi_2) = (l_1 \sin \phi_1, l_1 \cos \phi_1, \phi_2)$. The reconstruction image is then $\hat{\mathbf{x}} = (\hat{\mathbf{x}}_1, \dots, \hat{\mathbf{x}}_n)$, where $\hat{\mathbf{x}}_i = \text{STN}(\mathbf{x}_i^c, \mathcal{T}^{-1}(T_i^{\text{dec}}(\mathbf{q}, \mathbf{c})))$.

3.5 Loss function

The loss $\mathcal{L}(\mathbf{X})$ consists of the sum of three terms:

$$\mathcal{L}(\mathbf{X}) = \underbrace{-\mathbb{E}_{\mathbf{q}^0 \sim Q}[\log P(\mathbf{x}^0|\mathbf{q}^0)] + \text{KL}(Q(\mathbf{q}^0|\mathbf{x}^0)||P(\mathbf{q}^0))}_{\text{VAE loss}} + \underbrace{\sum_{\tau=1}^{T_{\text{pred}}} \|\hat{\mathbf{x}}^\tau - \mathbf{x}^\tau\|_2^2}_{\text{prediction loss}} + \lambda \underbrace{\sum_j \sqrt{\alpha_j^2 + \beta_j^2}}_{\text{vM regularization}}. \quad (16)$$

The VAE loss is a variational bound on the marginal log-likelihood of initial data $P(\mathbf{x}^0)$. The prediction loss captures inaccurate predictions of the latent Lagrangian dynamics. The vM regularization with weight λ penalizes large norms of vectors (α_j, β_j) , preventing them from blowing up.

⁴We use the reparametrization trick proposed by Davidson et al. [30] to sample from a von Mises distribution.

⁵For a transformation that depends on one or more generalized coordinate, those generalized coordinates must be encoded before the transformation can be applied. In the CartPole example, we need to encode r before applying the transformation to put the attention window centered at the cart to encode ϕ . We use the mean of the distribution, i.e., q_j^m or $(\cos q_j^m, \sin q_j^m)$, for those transformations that depend on q_j .

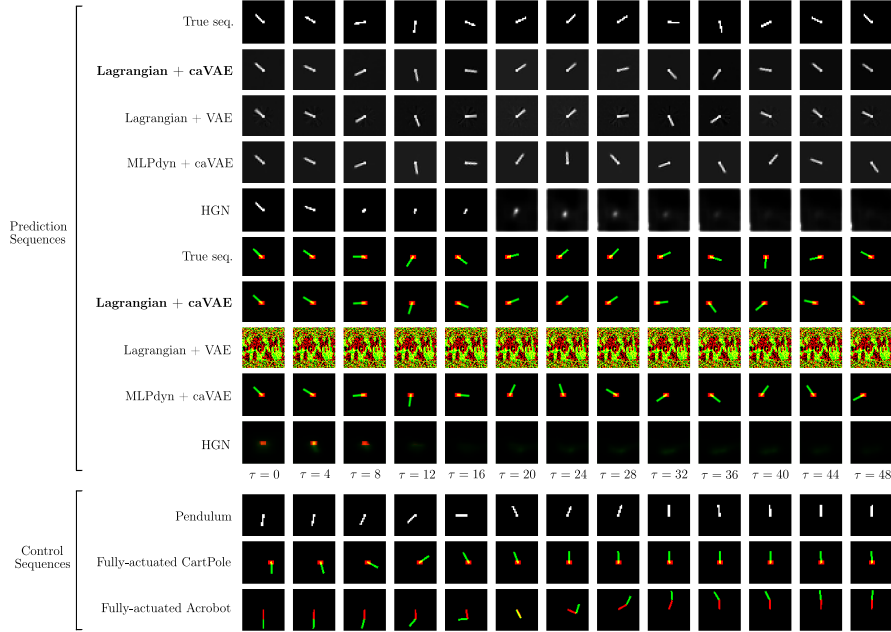


Figure 3: **Top:** Prediction sequences of Pendulum and CartPole with a previously unseen initial condition and zero control. Prediction results show both Lagrangian dynamics and coordinate-aware VAE are necessary to perform long term prediction. **Bottom:** Control sequences of three systems. Energy-based controllers are able to control the systems to the goal positions based on learned dynamics and encoding with Lagrangian+caVAE.

4 Results

We train our model on three systems: the Pendulum, the fully-actuated CartPole and the fully-actuated Acrobot. The training images are generated by OpenAI Gym simulator [33]. The training setup is detailed in Supplementary Materials. As the mean square error in the image space is not a good metric of long term prediction accuracy [8], we report on the prediction image sequences of a previously unseen initial condition and highlight the interpretability of our model.

Lagrangian dynamics and coordinate-aware VAE improve prediction. As the Acrobot is a chaotic system, accurate long term prediction is impossible. Figure 3 shows the prediction sequences of images up to 48 time steps of the Pendulum and CartPole experiments with models trained with $T_{\text{pred}} = 4$. We compare the prediction results of our model (labelled as *Lagrangian+caVAE*) with two model variants: *MLPdyn+caVAE*, which replaces the Lagrangian latent dynamics with MLP latent dynamics, and *Lagrangian+VAE*, which replaces the coordinate-aware VAE with a traditional VAE. The traditional VAE fails to reconstruct meaningful images for CartPole, although it works well in the simpler Pendulum system. With well-learned coordinates, models that enforce Lagrangian dynamics result in better long term prediction, e.g., as compared to *MLPdyn+caVAE*, since Lagrangian dynamics with zero control preserves energy (see Supplementary Materials).

Learned potential energy enables energy-based control. Figure 4 shows the learned potential energy of the three systems and reconstruction images at selected coordinates with *Lagrangian+caVAE*. The learned potential energy is consistent with the true potential energy of those systems, e.g., the pendulum at the upward position has the highest potential energy while the pendulum at the downward position has the lowest potential energy. Figure 4 also visualizes the learned coordinates. Learning interpretable coordinates and potential energy enables energy-based controllers. Based on the learned encoding and dynamics, we are able to control Pendulum and fully-actuated Acrobot to the inverted position, and fully-actuated CartPole to a position where the pole points upward. The sequences of images of controlled trajectories as shown in Figure 3 are generated based on learned dynamics and encoding with *Lagrangian+caVAE* as follows. We first encode an image of the goal position \mathbf{x}^* to the goal generalized coordinates \mathbf{q}^* . At each time step, the OpenAI Gym simulator of a system can take a control input, integrate one time step forward, and output an image of the system at the

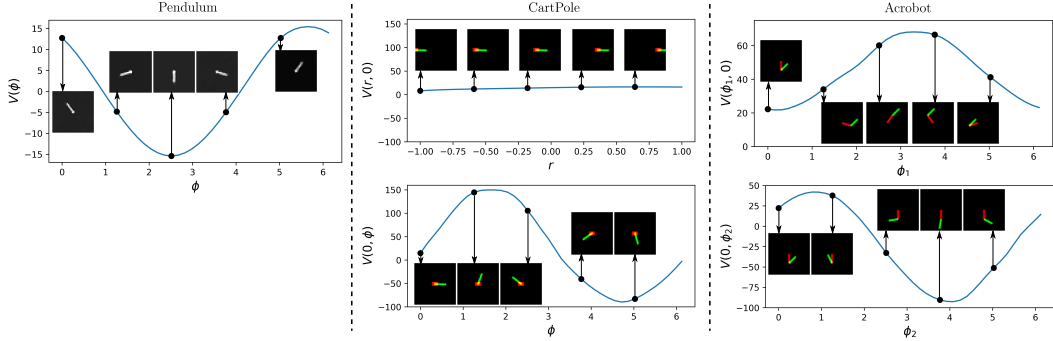


Figure 4: Learned potential energy with Lagrangian+caVAE of three systems and reconstruction images at selected coordinates. Both the learned coordinates and potential energy are interpretable.

next time step. The control input to the simulator is $\mathbf{u}(\mathbf{q}, \dot{\mathbf{q}}) = \boldsymbol{\beta}(\mathbf{q}) + \mathbf{v}(\dot{\mathbf{q}})$ which is designed as in Section 2.2 with the learned potential energy, input matrix, coordinates encoded from the output images, and \mathbf{q}^* .

Average pixel MSE	Pendulum (train test)		CartPole (train test)		Acrobot (train test)	
Lagrangian + caVAE	1.82	1.83	2.78	2.81	3.06	3.14
Lagrangian + VAE	1.52	1.56	9.41	10.30	10.48	10.78
MLPdyn + caVAE	1.92	1.92	14.18	14.97	12.12	12.14
HGN	0.55*	0.71*	2.81*	2.91*	2.61*	2.67*

Table 1: Average pixel MSE of different models. All values are multiplied by $1e+3$. The starred values are calculated from trajectories without control.

Baselines We set up two baseline models: HGN [6] and PixelHNN [3]. Neither model considers control input so we only use the trajectories with zero control in our dataset to train the models. Because of this, it is not fair to compare the pixel MSE of HGN in Table 1 with those of other models. We implemented HGN based on the architecture described in the paper and used the official code for PixelHNN. From Figure 3, we can see that HGN makes good predictions for the pendulum up to the training sequence length ($\tau = 4$), but makes blurry long term predictions. HGN fails to generalize to the test dataset for the CartPole task. This is probably because HGN is not data efficient. In the original HGN experiment [6], $30 \times 50K = 1.5M$ training images are used in the pendulum task, while here we use $20 \times 256 = 5120$ training images (with zero control). Moreover, the dimension of latent coordinate \mathbf{q} is $4 \times 4 \times 16 = 256$. With such a fixed high dimension (for various tasks), HGN does not need to assume degrees of freedom. However, it might not be easy to interpret the learned \mathbf{q} , whereas the learned coordinates in our model are interpretable. PixelHNN does not use an integrator and requires a special term in the loss function. PixelHNN does not account for the rotational nature of coordinate q , so the reconstruction images around the unstable equilibrium point are blurry and the learned coordinates are not easy to interpret (see Supplementary Material). In the original implementation of PixelHNN [3], the angle of the pendulum is constrained to be from $-\pi/6$ to $\pi/6$, where a linear approximation of the nonlinear dynamics is learned, which makes the learned coordinates easy to interpret. This constraint does not hold for more challenging control tasks.

Ablation study To understand which component in our model contributes to learning interpretable generalized coordinates the most, we also report results of four ablations, which are obtained by (a) replacing the coordinate-aware encoder with a black-box MLP, (b) replacing the coordinate-aware decoder with a black-box MLP, (c) replacing the coordinate-aware VAE with a coordinate-aware AE, and (d) a Physics-as-inverse-graphics (PAIG) model [14]. We observe that the coordinate-aware decoder makes the primary contribution to learning interpretable coordinates, and the coordinate-aware encoder makes a secondary contribution. The coordinate-aware AE succeeds in Pendulum and Acrobot tasks but fails in the CartPole task. PAIG uses AE with a neural network velocity estimator. We find that PAIG’s velocity estimator overfits the training data, which results in inaccurate long term prediction. Please see Supplementary Materials for prediction sequences of the ablation study.

5 Conclusion

We propose an unsupervised model that learns planar rigid-body dynamics from images in an explainable and transparent way by incorporating the physics prior of Lagrangian dynamics and a coordinate-aware VAE, both of which we show are important for accurate prediction in the image space. The interpretability of the model allows for synthesis of model-based controllers.

Broader Impact

We focus on the impact of using our model to provide explanations for physical system modelling. Our model could be used to provide explanations regarding the underlying symmetries, i.e., conservation laws, of physical systems. Further, the incorporation of the physics prior of Lagrangian dynamics improves robustness and generalizability for both prediction and control applications.

We see opportunities for research applying our model to improve transparency and explainability in reinforcement learning, which is typically solved with low-dimensional observation data instead of image data. Our work also enables future research on vision-based controllers. The limitations of our work will also motivate research on unsupervised segmentation of images of physical systems.

Acknowledgments and Disclosure of Funding

This research has been supported in part by ONR grant #N00014-18-1-2873 and by the School of Engineering and Applied Science at Princeton University through the generosity of William Addy '82. Yaofeng Desmond Zhong would like to thank Christine Allen-Blanchette, Shinkyu Park, Sushant Veer and Anirudha Majumdar for helpful discussions. We also thank the anonymous reviewers for providing detailed and helpful feedback.

References

- [1] Michael Lutter, Christian Ritter, and Jan Peters. Deep Lagrangian networks: Using physics as model prior for deep learning. In *International Conference on Learning Representations*, 2019.
- [2] Miles Cranmer, Sam Greydanus, Stephan Hoyer, Peter Battaglia, David Spergel, and Shirley Ho. Lagrangian neural networks. *arXiv e-prints*, art. arXiv:2003.04630, 2020.
- [3] Samuel Greydanus, Misko Dzamba, and Jason Yosinski. Hamiltonian neural networks. In *Advances in Neural Information Processing Systems 32*, pages 15379–15389, 2019.
- [4] Yaofeng Desmond Zhong, Biswadip Dey, and Amit Chakraborty. Symplectic ode-net: Learning Hamiltonian dynamics with control. In *International Conference on Learning Representations*, 2020.
- [5] Yaofeng Desmond Zhong, Biswadip Dey, and Amit Chakraborty. Dissipative symoden: Encoding Hamiltonian dynamics with dissipation and control into deep learning. In *ICLR 2020 Workshop on Integration of Deep Neural Models and Differential Equations*, 2020.
- [6] Peter Toth, Danilo J. Rezende, Andrew Jaegle, Sébastien Racanière, Aleksandar Botev, and Irina Higgins. Hamiltonian generative networks. In *International Conference on Learning Representations*, 2020.
- [7] Nicholas Watters, Daniel Zoran, Theophane Weber, Peter Battaglia, Razvan Pascanu, and Andrea Tacchetti. Visual interaction networks: Learning a physics simulator from video. In *Advances in Neural Information Processing Systems 30*, pages 4539–4547, 2017.
- [8] Matthias Minderer, Chen Sun, Ruben Villegas, Forrester Cole, Kevin P Murphy, and Honglak Lee. Unsupervised learning of object structure and dynamics from videos. In *Advances in Neural Information Processing Systems 32*, pages 92–102, 2019.

- [9] Tejas D Kulkarni, Ankush Gupta, Catalin Ionescu, Sebastian Borgeaud, Malcolm Reynolds, Andrew Zisserman, and Volodymyr Mnih. Unsupervised learning of object keypoints for perception and control. In *Advances in Neural Information Processing Systems 32*, 2019.
- [10] Alvaro Sanchez-Gonzalez, Victor Bapst, Kyle Cranmer, and Peter Battaglia. Hamiltonian graph networks with ode integrators. *arXiv e-prints*, art. arXiv:1909.12790, 2019.
- [11] Filipe de Avila Belbute-Peres, Kevin Smith, Kelsey Allen, Josh Tenenbaum, and J. Zico Kolter. End-to-end differentiable physics for learning and control. In *Advances in Neural Information Processing Systems 31*, pages 7178–7189, 2018.
- [12] Manuel Watter, Jost Springenberg, Joschka Boedecker, and Martin Riedmiller. Embed to control: A locally linear latent dynamics model for control from raw images. In *Advances in Neural Information Processing Systems 28*, pages 2746–2754, 2015.
- [13] Nir Levine, Yinlam Chow, Rui Shu, Ang Li, Mohammad Ghavamzadeh, and Hung Bui. Prediction, consistency, curvature: Representation learning for locally-linear control. In *International Conference on Learning Representations*, 2020.
- [14] Miguel Jaques, Michael Burke, and Timothy Hospedales. Physics-as-inverse-graphics: Unsupervised physical parameter estimation from video. In *International Conference on Learning Representations*, 2020.
- [15] Jannik Kossen, Karl Stelzner, Marcel Hussing, Claas Voelcker, and Kristian Kersting. Structured object-aware physics prediction for video modeling and planning. In *International Conference on Learning Representations*, 2020.
- [16] Nicholas Watters, Loic Matthey, Matko Bosnjak, Christopher P. Burgess, and Alexander Lerchner. Cobra: Data-efficient model-based rl through unsupervised object discovery and curiosity-driven exploration. *arXiv e-prints*, art. arXiv:1905.09275, 2019.
- [17] Peter Battaglia, Razvan Pascanu, Matthew Lai, Danilo Jimenez Rezende, and Koray Kavukcuoglu. Interaction networks for learning about objects, relations and physics. In *Advances in Neural Information Processing Systems 29*, pages 4502–4510, 2016.
- [18] Alvaro Sanchez-Gonzalez, Nicolas Heess, Jost Tobias Springenberg, Josh Merel, Martin Riedmiller, Raia Hadsell, and Peter Battaglia. Graph networks as learnable physics engines for inference and control. In *Proceedings of the 35th International Conference on Machine Learning*, volume 80, pages 4470–4479, 2018.
- [19] Steindor Saemundsson, Alexander Terenin, Katja Hofmann, and Marc Peter Deisenroth. Variational integrator networks for physically structured embeddings. *arXiv e-prints*, art. arXiv:1910.09349, 2019.
- [20] Danijar Hafner, Timothy Lillicrap, Ian Fischer, Ruben Villegas, David Ha, Honglak Lee, and James Davidson. Learning latent dynamics for planning from pixels. In Kamalika Chaudhuri and Ruslan Salakhutdinov, editors, *Proceedings of the 36th International Conference on Machine Learning*, volume 97, pages 2555–2565, 2019.
- [21] Marco Fraccaro, Simon Kamronn, Ulrich Paquet, and Ole Winther. A disentangled recognition and nonlinear dynamics model for unsupervised learning. In *Advances in Neural Information Processing Systems*, pages 3601–3610, 2017.
- [22] Danijar Hafner, Timothy Lillicrap, Jimmy Ba, and Mohammad Norouzi. Dream to control: Learning behaviors by latent imagination. In *International Conference on Learning Representations*, 2020. URL <https://openreview.net/forum?id=S110TC4tDS>.
- [23] Frederik Ebert, Chelsea Finn, Sudeep Dasari, Annie Xie, Alex Lee, and Sergey Levine. Visual foresight: Model-based deep reinforcement learning for vision-based robotic control. *arXiv preprint arXiv:1812.00568*, 2018.

- [24] Adam Paszke, Sam Gross, Francisco Massa, Adam Lerer, James Bradbury, Gregory Chanan, Trevor Killeen, Zeming Lin, Natalia Gimelshein, Luca Antiga, Alban Desmaison, Andreas Kopf, Edward Yang, Zachary DeVito, Martin Raison, Alykhan Tejani, Sasank Chilamkurthy, Benoit Steiner, Lu Fang, Junjie Bai, and Soumith Chintala. Pytorch: An imperative style, high-performance deep learning library. In *Advances in Neural Information Processing Systems* 32, pages 8024–8035, 2019.
- [25] William Falcon. Pytorch lightning. *GitHub. Note: <https://github.com/PyTorchLightning/pytorch-lightning>*, 3, 2019.
- [26] Romeo Ortega, Arjan J Van Der Schaft, Iven Mareels, and Bernhard Maschke. Putting energy back in control. *IEEE Control Systems Magazine*, 21(2):18–33, 2001.
- [27] Anthony M. Bloch, Naomi Ehrich Leonard, and Jerrold E. Marsden. Controlled lagrangians and the stabilization of mechanical systems. i. the first matching theorem. *IEEE Transactions on Automatic Control*, 45(12):2253–2270, 2000.
- [28] Ricky T. Q. Chen, Yulia Rubanova, Jesse Bettencourt, and David K. Duvenaud. Neural ordinary differential equations. In *Advances in Neural Information Processing Systems* 31, pages 6571–6583, 2018.
- [29] Diederik P. Kingma and Max Welling. Auto-encoding variational bayes. In *International Conference on Learning Representations*, 2014.
- [30] Tim R. Davidson, Luca Falorsi, Nicola De Cao, Thomas Kipf, and Jakub M. Tomczak. Hyper-spherical variational auto-encoders. *34th Conference on Uncertainty in Artificial Intelligence (UAI-18)*, 2018.
- [31] Eric Kauderer-Abrams. Quantifying translation-invariance in convolutional neural networks. *arXiv e-prints*, art. arXiv:1801.01450, 2017.
- [32] Max Jaderberg, Karen Simonyan, Andrew Zisserman, and Koray Kavukcuoglu. Spatial transformer networks. In *Advances in Neural Information Processing Systems* 28, pages 2017–2025, 2015.
- [33] Greg Brockman, Vicki Cheung, Ludwig Pettersson, Jonas Schneider, John Schulman, Jie Tang, and Wojciech Zaremba. OpenAI Gym. *arXiv e-prints*, art. arXiv:1606.01540, 2016.
- [34] Richard S Sutton. Generalization in reinforcement learning: Successful examples using sparse coarse coding. In *Advances in neural information processing systems*, pages 1038–1044, 1996.
- [35] Herbert Goldstein, Charles Poole, and John Safko. *Classical Mechanics*. American Association of Physics Teachers, 2002.
- [36] Louis N. Hand and Janet D. Finch. *Analytical Mechanics*. Cambridge University Press, 1998.

Supplementary Materials

S1 Summary of model assumptions

Here we summarize all our model assumptions and highlight what are learned from data.

Model assumptions:

- **The choice of coordinates:** we choose which set of coordinate we want to learn and design coordinate-aware VAE accordingly. This is important from an interpretability perspective. Take the Acrobot as an example, the set of generalized coordinates that describes the time evolution of the system is not unique (see Figure 5 in [34] for another choice of generalized coordinates.) Because of this non-uniqueness, without specifying which set of coordinates we want to learn will let the model lose interpretability.
- **Geometry:** this includes the using von Mises distribution for rotational coordinates and spatial transformer networks for obtaining attention windows.
- **Time evolution of the rigid-body system can be modelled by Lagrangian dynamics:** since Lagrangian dynamics can modelled a broad class of rigid-body systems, this assumption is reasonable and help us gain interpretability.

What are learned from data:

- **Values of the chosen coordinates:** although we choose which set of coordinates to learn, the values of those coordinates cooresponding to each image are learned.
- **Shape, length and mass of objects:** the coordinate-aware decoder learns the shape of the objects first and place them in the image according to the learned coordinates. The length of objects are modelled as learnable parameters in the model when those length need to be used (e.g. Acrobot). The mass of the objects are learned as $\mathbf{M}(s_1, s_2, s_3)$.
- **Potential energy:** this is learned as $V(s_1, s_2, s_3)$.
- **How control influences the dynamics:** this is learned as $\mathbf{g}(s_1, s_2, s_3)$.

S2 Conservation of energy in Lagrangian dynamics

In the following, we review the well known result from Lagrangian mechanics, which shows that with no control applied, the latent Lagrangian dynamics conserve energy, see, e.g., Goldstein et al. [35], Hand and Finch [36].

Theorem 1 (Conservation of Energy in Lagrangian Dynamics). *Consider a system with Lagrangian dynamics given by Equation (3). If no control is applied to the system, i.e, $\mathbf{u} = \mathbf{0}$, then the total system energy $E(\mathbf{q}, \dot{\mathbf{q}}) = T(\mathbf{q}, \dot{\mathbf{q}}) + V(\mathbf{q})$ is conserved.*

Proof. We compute the derivative of total energy with respect to time and use the fact that, for any real physical system, the mass matrix is symmetric positive definite. We compute

$$\begin{aligned} \frac{dE(\mathbf{q}, \dot{\mathbf{q}})}{dt} &= \frac{\partial E}{\partial \mathbf{q}} \dot{\mathbf{q}} + \frac{\partial E}{\partial \dot{\mathbf{q}}} \ddot{\mathbf{q}} \\ &= \frac{1}{2} \dot{\mathbf{q}}^T \frac{d\mathbf{M}(\mathbf{q})}{dt} \dot{\mathbf{q}} + \dot{\mathbf{q}}^T \frac{dV(\mathbf{q})}{d\mathbf{q}} + \dot{\mathbf{q}}^T \mathbf{M}(\mathbf{q}) \ddot{\mathbf{q}} \\ &= \dot{\mathbf{q}}^T \mathbf{g}(\mathbf{q}) \mathbf{u}, \end{aligned}$$

where we have substituted in Equation (3). Thus, if $\mathbf{u} = \mathbf{0}$, the total energy $E(\mathbf{q}, \dot{\mathbf{q}})$ is conserved. \square

With Lagrangian dynamics as our latent dynamics model, we automatically incorporate a prior of energy conservation into physical system modelling. This explains why our latent Lagrangian dynamics result in better prediction, as shown in Figure 3.

This property of energy conservation also benefits the design of energy-based controllers $\mathbf{u}(\mathbf{q}, \dot{\mathbf{q}}) = \boldsymbol{\beta}(\mathbf{q}) + \mathbf{v}(\dot{\mathbf{q}})$. With only potential energy shaping $\boldsymbol{\beta}(\mathbf{q})$, we shape the potential energy so that the system behaves as if it is governed by a desired Lagrangian L_d . Thus, the total energy is still conserved, and the system would oscillate around the global minimum of the desired potential energy V_d , which is \mathbf{q}^* . To impose convergence to \mathbf{q}^* , we add damping injection $\mathbf{v}(\dot{\mathbf{q}})$. In this way, we systematically design an interpretable controller.

S3 Experimental setup

S3.1 Data generation

All the data are generated by OpenAI Gym simulator. For all tasks, we combine 256 initial conditions generated by OpenAI Gym with 5 different constant control values, i.e., $u = -2.0, -1.0, 0.0, 1.0, 2.0$. For those experiments with multi-dimensional control inputs, we apply these 5 constant values to each dimension while setting the value of the rest of the dimensions to be 0. The purpose is to learn a good $\mathbf{g}(\mathbf{q})$. The simulator integrates 20 time steps forward with the fourth-order Runge-Kutta method (RK4) to generate trajectories and all the trajectories are rendered into sequences of images.

S3.2 Model training

Prediction time step T_{pred} . A large prediction time step T_{pred} penalizes inaccurate long term prediction but requires more time to train. In practice, we found that $T_{\text{pred}} = 2, 3, 4, 5$ are able to get reasonably good prediction. In the paper, we present results of models trained with $T_{\text{pred}} = 4$.

ODE Solver. As for the ODE solver, it is tempting to use RK4 since this is how the training data are generated. However, in practice, using RK4 would make training extremely slow and sometimes the loss would blow up. It is because the operations of RK4 result in a complicated forward pass, especially when we also use a relatively large T_{pred} . Moreover, since we have no access to the state data in the latent space, we penalize the reconstruction error in the image space. The accuracy gained by higher-order ODE solvers in the latent space might not be noticeable in the reconstruction error in the image space. Thus, during training, we use an first-order Euler solver. As the Euler solver is inaccurate especially for long term prediction, after training, we use RK4 instead of Euler to get better long term prediction results with learned models.

Data reorganization. As our data are generated with 20 times steps in each trajectory, we would like to rearrange the data so that each trajectory contains $T_{\text{pred}} + 1$ time steps, as stated in Section 3. In order to utilize the data as much as possible, we rearrange the data $((\tilde{\mathbf{x}}^1, \mathbf{u}^c), (\tilde{\mathbf{x}}^2, \mathbf{u}^c), \dots, (\tilde{\mathbf{x}}^{20}, \mathbf{u}^c))$ into $((\tilde{\mathbf{x}}^i, \mathbf{u}^c), (\tilde{\mathbf{x}}^{i+1}, \mathbf{u}^c), \dots, (\tilde{\mathbf{x}}^{i+T_{\text{pred}}}, \mathbf{u}^c))$, where $i = 1, 2, \dots, 20 - T_{\text{pred}}$. Now the length of each reorganized trajectory is $T_{\text{pred}} + 1$.

Batch generation. There are two ways of constructing batches of such sequences to feed the neural network model. The standard way is to randomly sample a certain number of sequences from the reorganized data. An alternative way is to only sample sequences from a specified constant control so that within each batch, the control values that are applied to the trajectories are the same. Of course, this control value would change from batch to batch during training. The reason behind this homogeneous control batch generation is the following. Except $\mathbf{g}(\mathbf{s}_1, \mathbf{s}_2, \mathbf{s}_3)$, all the vector-valued functions we parametrized by neural networks can be learned by trajectory data with zero control. From this perspective, all the trajectory data with nonzero control contributes mostly to learning $\mathbf{g}(\mathbf{s}_1, \mathbf{s}_2, \mathbf{s}_3)$. If this is the case, we can feed trajectory data with zero control more frequently and all the other data less frequently. All the results shown in the main paper and in the next section are trained with homogeneous control batch generation. We present the results of the standard batch generation in Section S5.

Annealing on weight λ . In Equation (16), the vM regularization with weight λ penalizes large norms of vectors (α_j, β_j) . In our experiments, we found that sometimes an annealing scheme such as $\lambda = \min(i_e/8000, 0.375)$ results in better reconstruction images than a constant weight, where i_e is the current epoch number during training.

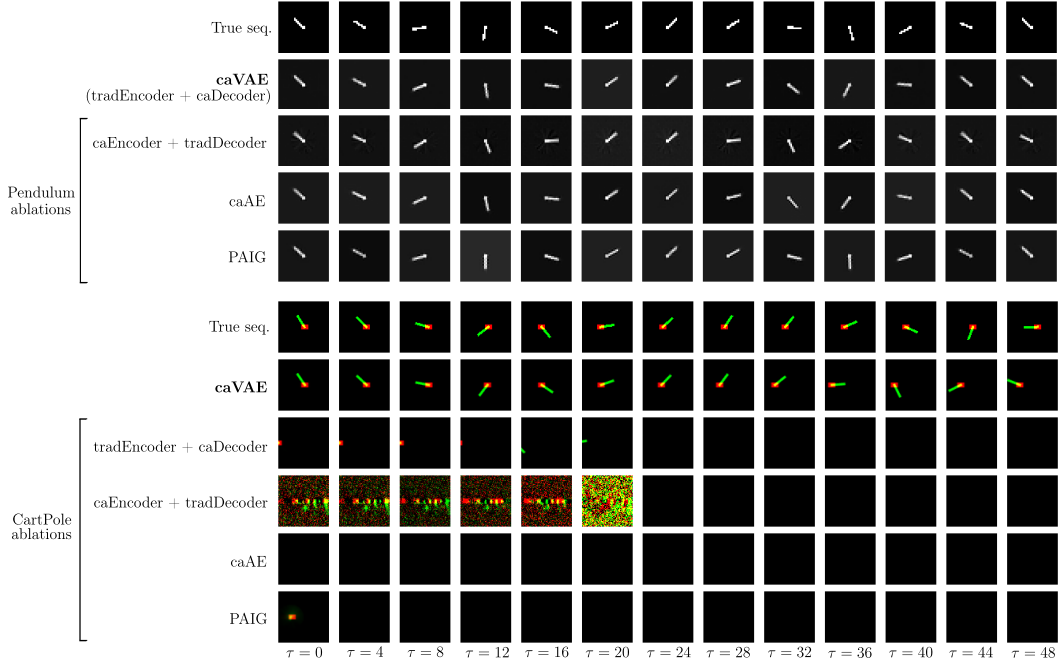


Figure 5: Prediction sequences of ablations of Pendulum and CartPole with a previously unseen initial condition and zero control. For the Pendulum experiment, the coordinate-aware encoder is a traditional MLP encoder. All the ablations get good predictions. For the CartPole experiment, all the ablations fail to get good predictions. The *PAIG* is able to reconstruct the cart initially but it fails to reconstruct the pole and make prediction. The *caAE* fails to reconstruct anything. The *caEncoder+tradDecoder* fails to reconstruct meaningful rigid bodies. The *tradEncoder+caDecoder* seems to extract meaningful rigid bodies but it fails to put the rigid bodies in the right place in the image, indicating the coordinates are not well learned.

Optimizer. For all the experiments, we use the Adam optimizer to train our model.

S4 Ablation study details

We report on the following four ablations:

- (a) **tradEncoder + caDecoder:** replacing the coordinate-aware encoder with a traditional black-box MLP
- (b) **caEncoder + tradDecoder:** replacing the coordinate-aware decoder with a traditional black-box MLP
- (c) **caAE:** replacing the coordinate-aware VAE with a coordinate-aware AE
- (d) **PAIG:** a Physics-as-inverse-graphics model

Figure 5 shows the prediction sequences of ablations of Pendulum and CartPole. Our proposed model is labelled as *caVAE*. Since long term prediction of the chaotic Acrobot is not possible, Figure 6 shows the reconstruction image sequences of ablations of Acrobot. From the results, we find that *PAIG* and *caAE* completely fails in CartPole and Acrobot, although they work well in the simple Pendulum experiment. By replacing the coordinate-aware decoder, *caEncoder+tradDecoder* fails to reconstruct rigid bodies in CartPole and Acrobot. By replacing the coordinate-aware encoder, *tradEncoder+caDecoder* reconstructs correct images with well-learned coordinates in Pendulum and Acrobot, but in CartPole, the coordinates are not well-learned, resulting in bad prediction. Thus, we conclude that the coordinate-aware decoder makes the primary contribution to learning interpretable generalized coordinates and getting good reconstruction images, while the coordinate-aware encoder makes a secondary contribution.

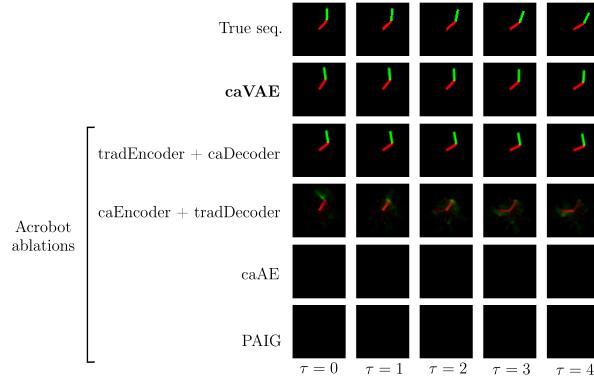


Figure 6: Reconstruction image sequences of ablations of Acrobot with a previously unseen initial condition and zero control. The *PAIG* and *caAE* fail to reconstruct anything. The *caEncoder+tradDecoder* fails to reconstruct the green link at all. The *tradEncoder+caDecoder* makes good reconstruction.

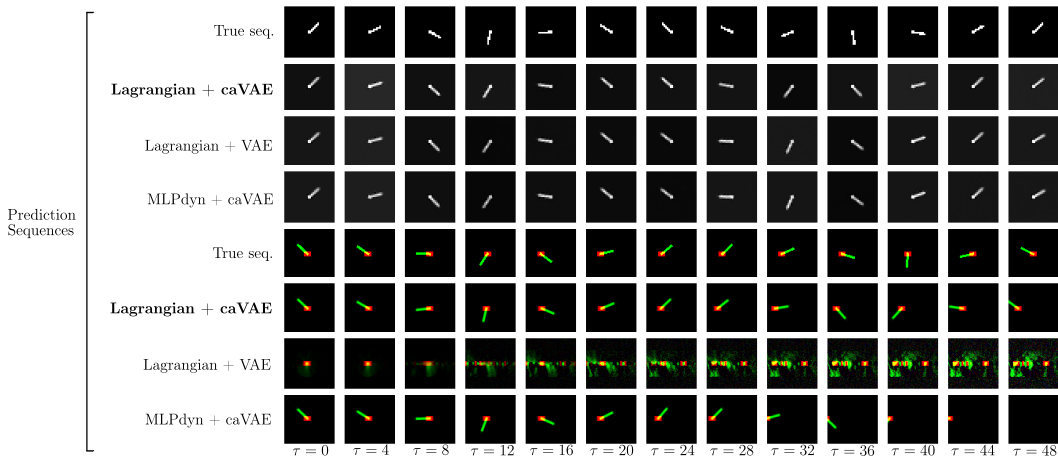


Figure 7: Prediction sequences of Pendulum and CartPole with a previously unseen initial condition and zero control, trained with standard batch generation, as explained in Section S3.2.

S5 Results with standard batch generation

From Figure 3 and Figure 7, we can see that our model behaves consistently well in prediction. In our experiments, we observe that our model trained with standard batch generation fail to learn a good model in the Acrobot example for the purpose of control. How the batch generation and annealing scheme affect the quality of learned model is not easy to investigate. We leave this to future work.

S6 Blurry reconstruction of PixelHNN

The original PixelHNN are trained with sequences of pendulum image data limited to a small angle range $[-\pi/6, \pi/6]$. Here we train the PixelHNN with randomly sampled angles as initial conditions. Figure 8 and Figure 9 shows the prediction results and the latent trajectory of image sequences. As we can see, the latent space does not have an interpretable shape as in the original implementation (see cell 6 at this link). The prediction sequences are blurry especially near the unstable equilibrium point.

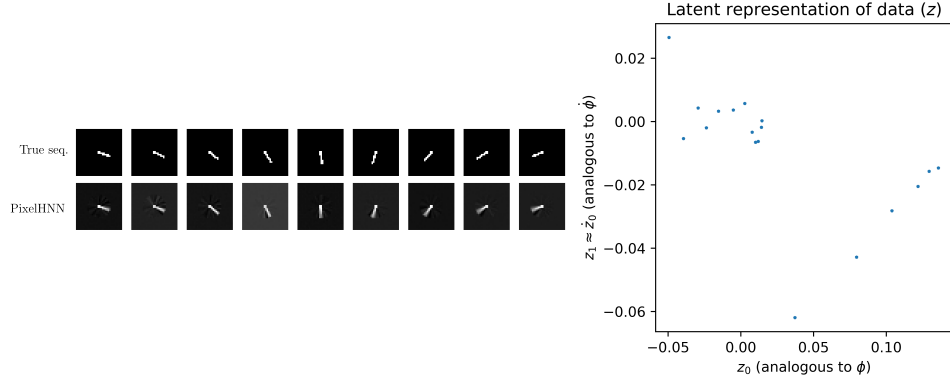


Figure 8: **Left:** True sequence and PixelHNN prediction of an initial position of the pendulum far away from the unstable equilibrium point. **Right,** the latent coordinate z and its time derivative \dot{z} of the PixelHNN prediction sequence.

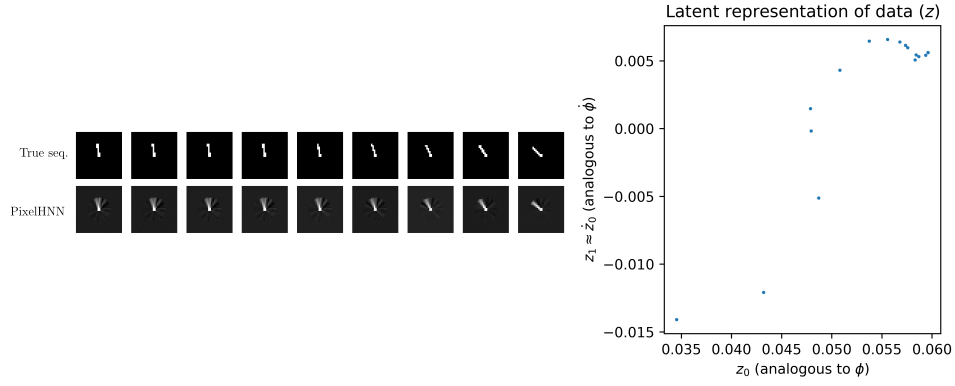


Figure 9: **Left:** True sequence and PixelHNN prediction of an initial position of the pendulum close to the unstable equilibrium point. **Right,** the latent coordinate z and its time derivative \dot{z} of the PixelHNN prediction sequence.

S7 Error in Equation (3)

In the previous versions of this paper

$$\frac{dM(\mathbf{q})}{dt}\dot{\mathbf{q}} \neq \frac{\partial}{\partial \mathbf{q}}(\dot{\mathbf{q}}^T M(\mathbf{q})\dot{\mathbf{q}}) \quad (17)$$

$$\dot{\mathbf{q}}^T \frac{dM(\mathbf{q})}{dt}\dot{\mathbf{q}} = \dot{\mathbf{q}}^T \frac{\partial}{\partial \mathbf{q}}(\dot{\mathbf{q}}^T M(\mathbf{q})\dot{\mathbf{q}}) \quad (18)$$